Unsteady Flow Simulation: A Numerical Challenge

Francesco Martelli, Elisabetta Belardini, Paolo Adami
Energetics Department Sergio Stecco
University of Florence
via S. Marta, 3
Florence-50139
Italy

ABSTRACT

The prediction of unsteady flow field in turbine blades as well as in the turbomachinery stages is now an affordable item, and is required by the reduced margin for increasing efficiency, stability and life of propulsion components. The numerical tools are now capable to run within reasonable time 3D unsteady calculation for full stage, and the new techniques on the computation and parallel computer allow the improvements of results in terms of cost and accuracy. Despite these advantages many questions remain open and the physical modelling joint with the numerical improvements is still a challenge if it has to produce usable results, compared with the experiments. On the other side the huge amount of data extracted from experiments require care and skinless to become useful tools for design. The two activities interact and support each other in the attempt to improve design quality. Aim of this paper is the report on some experience and the attempt to give some answer on that challenge, presenting results of a recent activity on modelling side compared with experiments as well. A full-3D unstructured solver based on an upwind TVD finite volume scheme has been developed and applied to the simulation of an unsteady turbine stage. The development of the numerical strategy is discussed with particular concern on the validation of the unsteady model through a comparison against experiments, NISRE approach and a 3D steady stage computation. The present work considers the application of the fully unstructured hybrid solver for internal viscous flows, as well. The multiblock version of the solver developed for turbine is considered, because of the highly improved performance as compared to the single domain version of the code. Moreover, the high numerical costs involved in 3D unsteady computations required the development of a new parallel single program multiple-data version of the numerical solver. The results compare favourably with a set of time averaged and unsteady experimental data available for the turbine stage under investigation, which is representative of a wide class of aero-engines.

Nomenclature

f,g,h	Convective fluxes
f	Frequency
J	Implicit residual Jacobian
Q	Conserved variables vector
p	Static pressure
$P0,T0$	Total pressure and temperature
R	Residual vector
S	Source term residual
t	Physical time
V	Element volume
s	Curvilinear abscissa
W	Mass flow rate
x,y,z	Space coordinate
W	Mass flow rate

Greek symbols

ρ	Density
τ	numerical time
ω	Rotational speed

Subsripts

1,2,3	NGV inlet, interstage and rotor outlet planes

Acronymous

GMRES	Generalised Minimal Residual Method
ILU	Incomplete LU factorisation
NISRE	Not Isoentropic Simple Radial Equilibrium
PE	Processing Element of a Parallel Architecture

Paper presented at the RTO AVT Symposium on "Reduction of Military Vehicle Acquisition Time and Cost through Advanced Modelling and Virtual Simulation", held in Paris, France, 22-25 April 2002, and published in RTO-MP-089.

1. INTRODUCTION

Computational Fluid Dynamics (CFD) has become an effective tool in the analysis of complex flows and the design of more efficient machinery components, thanks to its versatility in the investigation of different working conditions and to the capability in analysing overall and detailed information about the flow. The simulation of a transonic turbine stage requires both efficiency and accuracy in order to forecast the stage performances and the realistic representation of the unsteady stator/rotor interaction. In this regard many applications of structured codes for 3D turbine investigations have been reported in literature.

A basic assessment considering the research activity and the main impact of unsteadiness phenomena is given by Sharma et al., (1992). Among all the approaches proposed some authors use implicit ADI factorisation schemes for the simulation of quasi-3D stator-rotor interaction, while others apply an explicit multi-grid technique. Both the unsteady approaches are based on a dual-time stepping extension of the basic time marching procedure developed for steady state computations. Giles, (1990) describes a similar numerical scheme with the application of a different approach for a generic not even stator-rotor blade count ratio. A recent work of Dorney *et al.* (1997), compares accuracy and efficiency of different predicting models with increasing complexity, ranging from fully unsteady simulations to loosely coupled methods, for stage performances prediction. Other computational studies for turbine row interaction have been carried out by several authors among which Haa et al. (1993), Gallus et al. (1994), Dawes (1994), He (1996) and Walraevens *et al.* (1998). More recently von Hoyningen-Huene and Jung, (2000) have reported the application and comparison of different unsteady approaches for structured grids. The comparison considers an explicit method, a time consistent multi-grid and a dual-time step with multi-grid on structured grids.

A common drawback of all the structured approaches is the crude way required to improve accuracy in confined region of rapid gradient which also implies a costly grid refinement in a large, and not necessary, portion of the flow domain. A more sensible approach would instead refine the mesh locally only in regions where a sharp variation of the solution is expected. The first examples of unstructured codes for compressible simulations come from the external aerodynamics while more recently viscous extensions have been reported by Kwon and Hah, (1995) and Mavriplis, (1995). The more rational mesh refinement and the higher geometrical flexibility are the most attractive aspects of the unstructured approaches, allowing complex configurations to be represented and easily handled by the solution algorithm.

The main drawback is, undeniably, the high CPU and memory demand, which can rapidly waste the advantages offered by the increased geometrical flexibility. In this regard very few general applications have been documented in literature on the use of unstructured solvers for unsteady stator rotor interaction. An example is reported by Sayma *et al.* (2000), using semi-structured grids with a dual time step approach. A different strategy is proposed by Rai (1989) aiming to improve the geometrical flexibility through the use of patched structured grids.

The present work considers the application of a fully unstructured hybrid solver (HybFlow, Adami *et al.* 1998) for internal viscous flows. The multiblock version of the solver developed for turbine rows (Adami et al., 2000) is considered, because of the highly improved performance as compared to the single domain version of the code. Moreover, the high numerical costs involved in 3D unsteady computations required the development of a new parallel single program multiple-data version of the numerical solver. This improved version of HybFlow is applied to the simulation of the BRITE HP turbine stage experimentally tested in the compression tube facility CT3 of the Von Karman Institute (Dénos *et al.* 1999, 2000).

2. THE GOVERNING EQUATIONS

The basic numerical scheme of HybFlow code solves the compressible Navier-Stokes equations cast in strong conservative form (Adami, 1998). For the simulation of the flow field conditions inside turbine rotor rows, the conventional condensed formalism has been adopted:

$$\frac{\partial Q}{\partial t}+\frac{\partial f}{\partial x}+\frac{\partial g}{\partial y}+\frac{\partial h}{\partial z}=S \tag{1}$$

The governing equations have been extended to cope with a moving frame of reference rotating together with the rotor row. The same formalism of governing equations can be retained for both the fixed and the rotating frame adding the centrifugal and Coriolis terms in *S,* provided that, when applied to the rotor row, the velocity vector and all total quantities are referred to the relative frame (Belardini *et. al* 2000). The perfect gas state equation is finally used for the closure of the mathematical model.

3. THE NUMERICAL METHOD

The spatial discretization

The solver HybFlow is specialised for the computation of internal compressible/incompressible flows with and without chemical reactions. A brief description of the basic numerical scheme follows, while more details can be found in Adami *et al.* 1998, Adami *et al.* 2000, Belardini *et. al.* 2000. The spatial discretization is based on a finite volume approach for hybrid unstructured grids. Roe's approximate method is used for the upwind scheme. A linear reconstruction of the solution inside the elements provides a second order discretisation, and monotonicity is ensured through the TVD slope limiter proposed by Barth, (1991).

Two possible time accurate discretization are available:

- ◊ The explicit approach; the time accurate solution is computed using a five-step multi-stage Runge-Kutta scheme, with the classical scheme.
- ◊ The implicit dual-time stepping discretization;

The dual-time stepping approach adds an extra numerical time derivative to the physical unsteady equation (1):

$$\frac{\partial Q}{\partial \tau}+\left[\frac{\partial Q}{\partial t}+R(Q)-S(Q)\right]=0 \tag{2}$$

The physical time derivative can be expressed using a second order back-ward finite difference:

$$\left.\frac{\Delta Q}{\Delta t}\right|_{phys}^{(k)}=\frac{3Q^{(k)}-4Q^{n}+Q^{n-1}}{2\Delta t}$$

A classical time marching approach is then recovered to drive to convergence the numerical unsteady term. The time marching procedure is based on the approximate implicit Newton method for systems of non-linear equations. The physical time derivative is discretized with second order backward approximation and, collecting together the terms of the implicit Jacobian matrix, the classical formalism of the implicit method is recovered as follows:

$$\left\{\frac{I}{\Delta \tau}+J^{*}(Q^{(k)})\right\}\Delta Q^{(k)}=R^{*}\left(Q^{(k)}\right)$$

where

$$J^*\left(Q^{(k)}\right)=\frac{\partial}{\partial Q}\left[\left.\frac{\Delta Q}{\Delta t}\right|_{phys}^{(k)}+R(Q^{(k)})-S(Q^{(k)})\right]$$
$$R^*\left(Q^{(k)}\right)=-\left[\left.\frac{\Delta Q}{\Delta t}\right|_{phys}^{(k)}+R\left(Q^{(k)}\right)-S\left(Q^{(k)}\right)\right] \quad (3)$$

When the selected convergence criterion is satisfied $\Delta Q^{(k)} \approx 0$ and the physical solution at time level $n+1$ is updated: $Q^{n+1}=Q^{(k)}$

Stability of the numerical algorithm is provided by the time-marching relaxation term appearing in the implicit operator and resulting from the numerical time derivative $I/\Delta\tau$. The matrix of the implicit method is computed numerically by finite differences expressions of the residual vector R with respect to the solution (see Adami, 1998), while the contribution from the source terms is computed through analytical derivatives of S. The linear system stemming from equation (3) is solved at each integration step by the same iterative method GMRES (Saad, 1994) used for the steady state simulations. The efficient convergence of the linear solution requires preconditioning. The preconditioning matrix is computed performing an incomplete ILU(0) factorisation of the implicit matrix (Saad, 1994). It is worthwhile remembering that the whole procedure GMRES-ILU(0) makes use of a condensed storage format which accounts for matrices with non-zero elements only.

As proved in Fig. 1-a the implicit dual time stepping strategy shows an effective behavior in terms of robustness and stability. In fact the numerical time marching converges to the unsteady physical solution within 10 numerical sub-iterations with about 3 orders reduction of the initial residuals.

4. THE PARALLEL MULTI-BLOCK APPROACH FOR STAGE COMPUTATIONS

The multi-block and parallel strategy

Although basic solver provides an accurate description of internal flows at different Mach numbers, when dealing with complex geometry the simulation can require high CPU time and memory storage. A significant memory saving and reduction of the overall CPU cost has been obtained by means of different numerical tools. Firstly a multi-block strategy implementation allowed a significant reduction of memory usage, thanks to the reduced dimensions of the linear system matrix during the implicit marching of the solution. The multiblock approach had a positive effect on computing time also. In spite of the loss in robustness of the solver due to the additional new internal explicit boundaries created, the overall computational cost is considerably reduced.

Besides the domain decomposition technique represented an essential step, in view of the implementation of the code on parallel architectures. The parallel version of the code is based on the standard MPI message passing libraries to ensure high portability. The neighbouring elements residing on the local memory of different CPUs require the explicit activation of a communication procedure among processors to satisfy the physical flow continuity. The increase in the number of processors leads to a considerable decrease of computational costs. Nevertheless, communications amongst different processors represent a computational overhead, which can grow rapidly with the number of processors involved if the computational activity is incorrectly shared.

The present parallel approach distributes individual portions of the overall grid among different CPUs (data partitioning). In this case all processors perform the same set of operations solving the flow field inside the sub-domains assigned to each CPU: the distribution strategy, aimed to guarantee almost the same number of elements inside each block and a quite uniform distribution of blocks to different Pes, thus allowing a global load balancing.

In this regard the histogram of Figure 1 reports the early time profiling of the parallel solver (percentage of the different computational activities with respect to the total CPU time), during the solution of a test case. The test run on 16 processors on CINECA Origin 3800, a shared memory multiprocessor system based on Processing Elements (PEs) R12000 running at 400 MHz. Although physically distributed, the memory can be logically shared by the hardware able to address a unified global space.

In the porting of scalar solvers to parallel architectures a crucial feature in the estimation of code performance is the communication cost which is strictly related to the structure of the code and the algorithm. Usually for an implicit solver the system matrix storage and inversion require around 75÷80% of the total computational time. During this time the algorithm does not require inter-processor communications.

Early analysis of the scalar solver performance showed that, despite the use of efficient numerical strategies and of a compact storage method (Adami *et al.*, 1998), the implicit system required about 88% of the code memory demand. Overall, the time spent for residuals assembly and system matrix inversion was more than 90% of the total elapsed time. A more recent profiling of the parallel solver shows that matrix inversion is still the most time consuming activity requiring about 65% of the global CPU time, followed by communications (15%), flux assembly and I/O management. The distribution of these percentages is obviously dependent from the particular processor but the maximum difference remained below 3% demonstrating an acceptable load repartition. In view of these features of the solver all the optimisation strategies performed on the parallel code were mainly focused on the reduction of system inversion CPU time and communication strategy Among these the use of the most advanced compilers options (such as the better exploitation of pipeline mechanism, fast improved math libraries and the optimisation of the cache use) brought a 16% global CPU time reduction on numerical experiments performed in simpler configurations. Beside the Fortran routines managing the message passage MPI standard where implemented with the introduction of Fortran 90 dynamic allocation to reduce the dimension of the data packages to be sent or received during communications. This allowed another 3% CPU time reduction on a local 4 CPUs workstation. A different storage of system matrix lead to a limitation of global primary 'cache miss' and thus a further 6% reduction of the global CPU time.

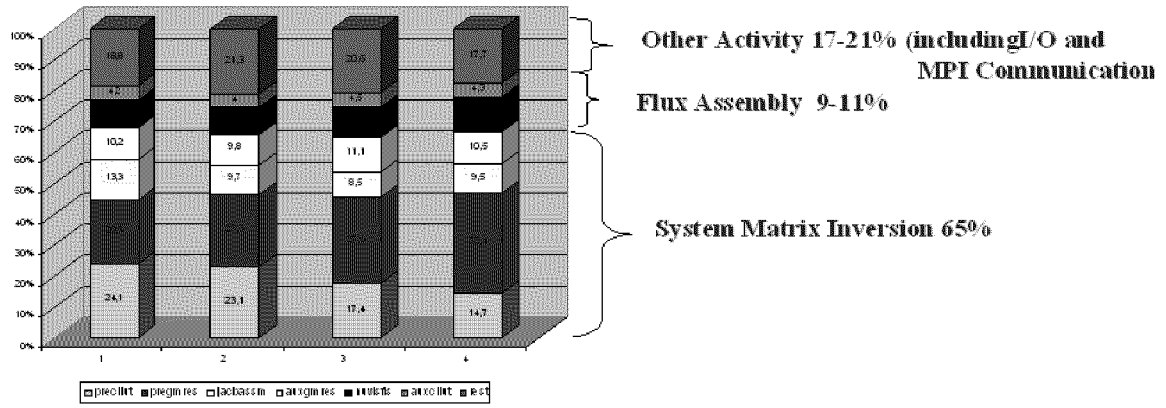

Figure 1 Time Profiling of the Solver on 16 CPU

To face the greater and greater dimensions of the flow problems and the management and storage of the amount of the data involved, attention can not be focused only on the optimisation of the flow solver itself but should take into account even all the routines of the so called pre and post-processing phases which had to be revised and improved. In this respect Figure 2 reports the main phases of a multi stage CFD computation which starts from the solid modelling and grid generation of the single stator and rotor rows using commercial software (Centaur^{TM}). The complete grid geometry of the stage is then assembled in a unique domain which is divided in smaller blocks trough a fully automatic domain decomposition technique (see Fig. 2). Finally the multiblock domain is distributed amongst the different processors and the processing of the data for unsteady

computation is performed (*Parallel and unsteady treatment* in Fig. 2). At this point the inlet data set is ready for the CFD simulation which will produced the basic flow features at various time steps of the simulation. Finally the data produced will be processed and synthesised to produce variables easy to be understood and interpreted to capture the basic flow physics of the problem such as time averaged pressure on the blade surface, unsteady pressure fluctuation in some interesting points or for the comparison with experimental data, pitch -wise time averages for secondary flow description and movies. With simpler flow configurations the pre and post processing phases where not critical but with the increasing of the problems dimension all these routines had to be revised and improved. In fact with increasing grid dimensions the CFD solver is surprisingly not the crucial phase of the whole approach while the most memory demanding step is the domain decomposition and the most CPU intensive step is the computing of unsteady information for the sliding mesh nterface (see next paragraph). The reason for this behaviour can be explained remembering that with increasing grid dimensions a larger CPU's cluster may be used to tackle the computational cost increase during the CFD application having a fully parallel structure. Conversely the same does not hold for the pre and post processing routines which naturally retain a scalar character required to manage the whole physical domain.
This problems has been presently reduced, keeping the same structure of the pre processing routines, with a proper use of the memory space through the Fortran 90 standard which allows a flexible dynamic memory allocation and de-allocation of unused matrices. With regard to the unsteady treatment the main problem was represented by the length of the interpolation searching techniques which required more than 48 hours to complete the final set up of the data for the unsteady simulation of the viscous grid made of 1.8M elements. In this case a more efficient searching strategy for the interpolation technique and a rationale use of the I/O management have been introduced to obtain a significant reduction of total required time (about ten times).

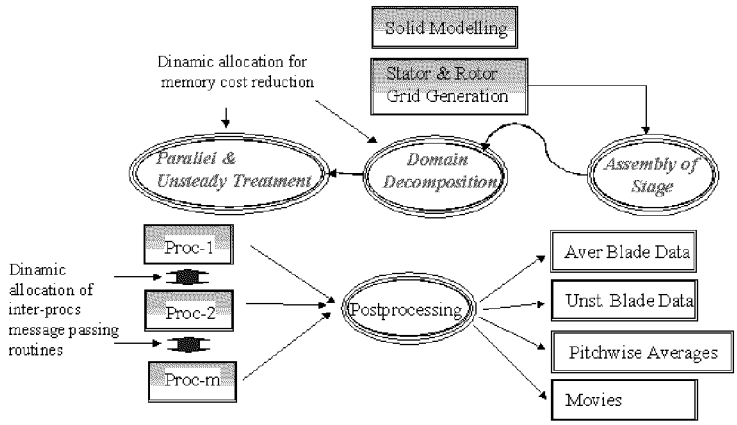

Figure 2: Pre and Post ProcessingTreatment

Boundary Conditions Sliding Interface

Inlet conditions are given at the stator inlet plane using the nominal total pressure and total temperature profiles as also the inlet flow angle. In the exit plane, hub static pressure is imposed and the radial equilibrium equation is applied to evaluate the static pressure distribution assuming an axially developed flow field. Solid surfaces are assumed to be adiabatic with zero normal mass and momentum fluxes. Periodicity is ensured with an exact point to point correspondence between elements belonging to the periodic boundaries. On the rotor stator interface a local interpolation has been developed to account for the relative rows movement and for the change of reference frame.

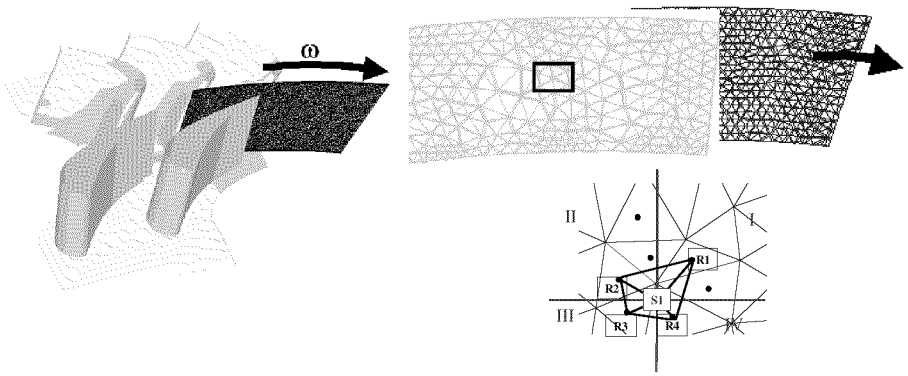

Figure 3: Interpolation Strategy in Sliding Interface

The grid close to the rotor-stator boundary is fully three-dimensional and unstructured to allow simple and efficient grid generation in the inter-stage gap. Thus, elements with triangular and quadrilateral faces from both stator and rotor grids need to be interfaced at varying angular positions (Figure 3). In such situations, the map of neighbouring elements and the definition of a simple matching strategy for the two rows poses serious difficulties, also because of the continuous displacement of the two moving blades during the unsteady computation. This geometrical problem has been overcome by the implementation of a crude, but general interpolation scheme between the two rows, as summarised in Figure 3. The interpolation strategy guarantees the continuity of static variables (density, pressure and temperature), while velocity components are discontinuous, according to the relationships between absolute and relative frames. Although the present method is not strictly conservative, the computations revealed that the mass imbalance is always well below 1%. A substantial reduction in the computing time to complete the full unsteady simulation (made up of several periodic revolutions), can be obtained with the storage of all information pertaining to the sliding interface interpolation in a look-up table accompanying the grid file. In this way the parameters for corresponding time periodic positions can be computed once for all time steps, avoiding time-consuming recalculations.

Grid Sequencing Strategy

In a CFD simulation usually an initial guess solution is used to start the computation. This rough solution is updated till the solver reaches the final exact numerical solution of the physical problem. When a complex domain and different physical aspects are involved, such as coolant injection mixed with the coupling of rotating and stationary parts, rarely this initial guess solution can be chosen close to the real one and thus stability problems may arise while several time steps can be required before the final convergence is obtained.

The number of this numerical steps has been strongly reduced, mainly in the viscous computation, using the grid sequencing strategy. The basic idea beyond this method is the creation and use of a family of grids with progressively increasing element number. An unsteady unviscous computation can be performed on the coarser grid to capture the fundamental flow physics or the basic frequency spectrum of the unsteady pressure fluctuations which are both almost independent from viscous phenomena. In the present application the coarse unviscid grid is made up of 360000 elements, of which 24000 on blade surface and 5700 on the sliding surface dividing the NGV from the rotor rows.

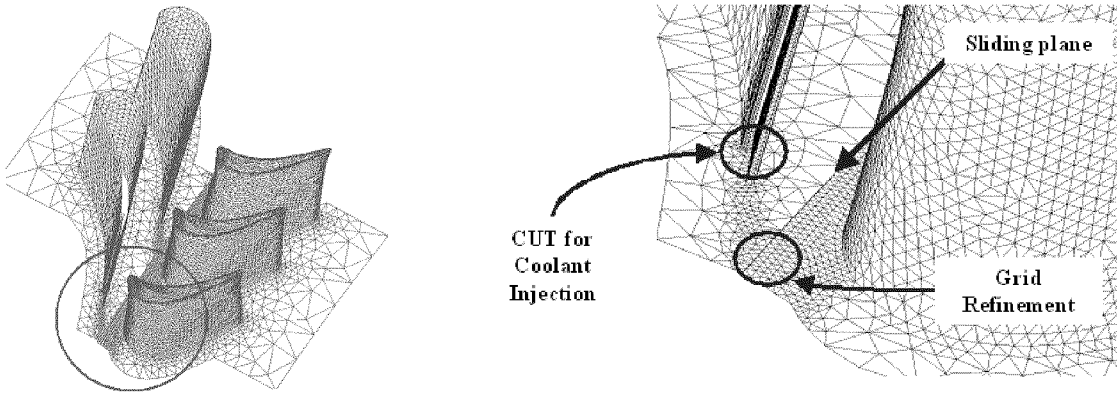

Figure 4. Coarse Grid for Unviscid Computations

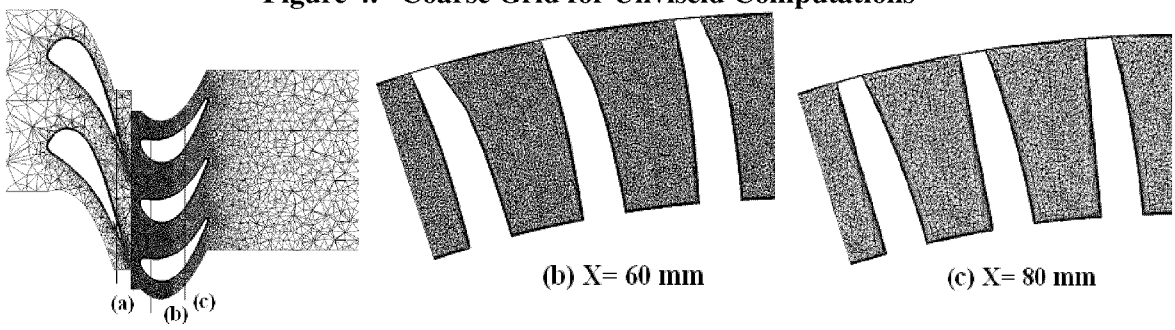

Figure 5: Refined Grid for Viscous Computations

The final converged numerical solution for unviscid simulation still requires a large number of steps but the CPU time is reduced in view of the smaller dimensions of the grid. Once the solution is obtained on the coarse grid a viscous and turbulent computations can be carried out on the second refined grid (Figure 4a) to capture the effect boundary layers development on the performance and efficiency of the stage. The initial guess solution can be represented by the unviscid solution obtained on the coarse grid which can be transferred to the refined simulation through an automatic grid adaptation technique. A general unstructured 3D routine has been ad hoc developed to interpolate the solution from the coarse to the second refined grid which is reported in Figure 4. A further refinement step has then performed using a third viscous grid shown in Figure 5. Grid refinement is evident in the radial section at midspan (Figure 5) where 10 prismatic layers have been introduced all around the NGV and rotor blade surfaces to capture the basic features of the boundary layer. Node elements have been also added in the rotor vane passage flow and mainly in the coolant injection area (slide (a) in figure 5) of the NGV which is thought to be responsible, together with the shock detaching from the TE of the stator blade, for the unsteady pressure fluctuations measured on the rotor blade. A strong grid refinement is also applied all over the pitch-wise direction ahead the rotor blade (slide (b)) in order to accurately capture the effect of the NGV wake for all relative positions of the two rows. Numerical computations performed demonstrated that this refinement requires a soft smoothing toward the trailing edge of the rotor to avoid the effect of the grid sensitivity of the solution on the different sizes of neighbouring cells which can strongly affect the accuracy/stability of the flow solution. Despite the refinement the global grid has a still feasible number of elements (1.8 Ml elements, 41000 on solid surfaces and 20000 on the sliding plane) owing to the high flexibility of the unstructured approach.

5. APPLICATION TO THE 3D VKI ANNULAR STAGE

Stage description

The present investigation is carried out on the first stage of the HP turbine with prismatic stators and fully three-dimensional rotor selected in the frame of the TATEF project. The project is devoted to gain a better understanding of the stator-rotor interaction phenomena for transonic annular

cascades. A brief description of the cascade is presented here, while more details about the experimental test rig and the data can be found in Denos et al. 1999.

A detailed measurement campaign provides data in several different operating conditions. In the present work nominal unsteady flow field conditions will be analysed. The main mid-span parameters of the test case at the nominal pressure ratio and for the nominal reference Reynolds Number ($\approx 10^6$) are:

Mis(exit NGV)=1.08, M(exit rotor)=0.42.

Cooling air injection is provided in the experimental configuration at the nozzle trailing edge through a pressure side cut of the blade..

Numerical simulation

The 3D unstructured grid topology used to perform the in viscid numerical simulation is shown in figure 4. Applying a slight stretching (about 0.8%) to the rotor vane geometry, an exact pitch ratio is obtained using 2 stator blades and 3 rotor blades. This modification to the geometry was positively tested by Michelassi et al. (1999).

The unviscid and viscous (first refinement) computations have been performed using the parallel version of the code on a cluster of four DEC ALPHA-XP1000-666 Mhz workstations. The coarse unviscid grid has been divided using 24 blocks equally distributed amongst the 4 CPUs with a memory request of the implicit procedure of 55 Mb.

The unsteady periodic solution has been reached starting from the rest condition and keeping the rotor blades fixed. The starting static pressure distribution has been established using a linear law between the inlet prescribed total pressure and the outlet measured static pressure. During the computation the rotating speed of the blades is gradually increased until the nominal velocity of 6500 RPM is reached in a physical period (three rotor passages). The physical time step is computed by dividing the natural periodic angle in a suitable number of steps able to guarantee both stability of the numerical procedure and an acceptable time resolution of the unsteady frequencies. The physical time, required to complete an entire period of the whole domain, can be easily computed from the ratio $\alpha/\omega = 2.88*10^{-4}\ s$ where ω is the rotational speed and α is the periodic angle (16.744 Deg). The nominal total quantities are used as boundary conditions at the NGV inlet assuming flat profiles for both T0 and P0. For the coolant jet, inlet conditions are set in order to match a global mass flow rate as observed in the experimental tests. At the outlet of the stage the integral value of the nominal experimental outlet static pressure is imposed.

In this regard one hundred steps per subdivision for the periodic pitch seemed enough to guarantee the accuracy of the unsteady solution and to capture the first main frequencies of the unsteady flow. The numerical time marching convergence of each unsteady physical solution can be achieved within 10 numerical sub-iterations with a reduction of the initial residuals larger than 4 orders of magnitude. The unsteady flow field converges to a pattern periodic in time after five complete passages of 2 stators and 3 rotors vanes. The viscous solution has been obtained starting from the solution obtained from the in viscid computation using the grid sequencing strategies and the ad hoc interpolation technique previously mentioned.

The computations have been performed with the same solver but using 16 processors on CINECA Origin 3800. The grid has been divided in about 400 blocks distributed amongst the 16 processing elements and two hundred steps have been chosen to complete the periodic passage. The number of sub iteration is 10 while the unsteady flow field converged to a new periodic pattern in time after 3 complete passages.

Results and discussion

Inviscid results

Once the periodic solution is achieved for the unsteady numerical computation, an overall mass error less than 1% has been observed from the stage inlet and outlet sections.

Hub and tip static pressure profiles are measured in the test rig at a station placed 0.035 axial chords downstream the nozzle trailing edge, using both Kulite transducers and static pressure taps

(Denos *et al.*, 1999). The instantaneous numerical pressure profiles have been time averaged both at hub and tip and compared against measurements in Figure 6 for a NGV blade pitch.

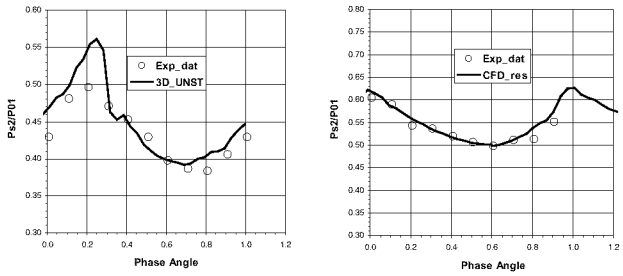

a) hub wall b) tip wall

Figure 6: hub and tip time-averaged pressure profiles

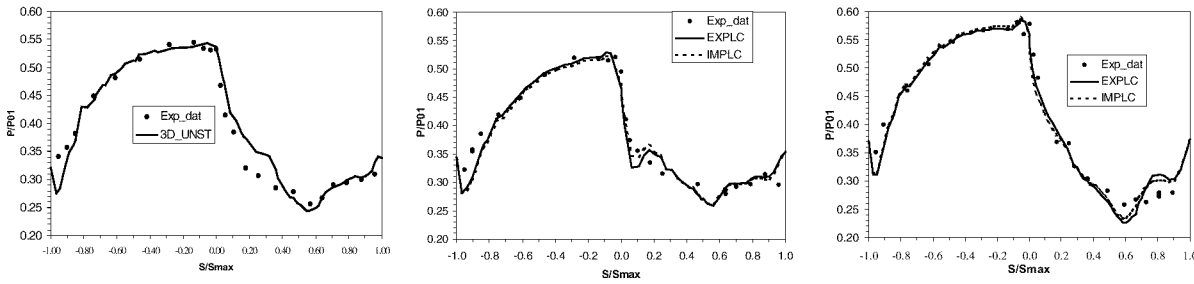

a) Averaged rotor pressure - 50% span b) Averaged rotor pressure - 15% span c) Averaged rotor pressure - 85% span

Figure 7: Time averaged Pressure Profiles

Moving from 0 to 1 along the abscissa, the measuring points move from the pressure side towards the suction side of the nozzle blade. Fig. 6 indicates a quite correct estimate of the average inter-stage working pressure in the numerical simulation. The steep pressure rise observed for the phase value around 0.2 can be explained by the over estimation of vane trailing shock intensity in the numerical computation caused by the absence in the calculation of viscous effects. This behaviour is more pronounced near the hub surface where the inviscid assumption is expected to give a less accurate prediction in view of the more relevant role played by the boundary layer thickness on the lower wall contouring. The time-averaged pressure profiles on the rotor blade are reported in Figure 7, for three radial sections at 50%, 15% and 85% of the blade span. In these figures static pressure over stage inlet total pressure is plotted against curvilinear abscissa on the rotor surface (positive/negative values indicate respectively locations on the suction/pressure side).

The agreement with experiments is satisfactory on the pressure side, while on the suction side and close to s/smax=0.2, the flow acceleration is slightly under predicted. This might indicate either a three-dimensional effect or a slight underestimation of the incidence (see Michelassi et al. 1999, 2001). The pressure rise and the shock location is correctly captured for s/smax=0.6.

At the 15% section close to the hub the computed pressure profile agrees closely with the experiments except for s/smax=0.1 on the suction side. In this location it is argued that the strong shock detaching from the stator trailing edge interacts with the rotor blades suction side giving the observed pressure rise on the rotor surface.

The instantaneous views of wall pressure patterns, indicate that the flow on the LE of the suction side may periodically undergo a strong acceleration, followed by a recompression shock in correspondence of some relative positions. For other phase angles, the flow pattern is quite different, and the same acceleration/compression pattern is not detected. A similar pattern can be detected close to tip, although slightly smeared with respect to the 15% section. This effect is responsible for the steep pressure rise shown by the hub averaged pressure comparison of Figure 7.

The near tip region pressure field of figure 7 reveals a stronger acceleration of the flow on the suction side close to the rotor trailing edge (s/smax=0.6). This over expansion is followed,

downstream the minimum value, by the pressure rise typical of a recompression shock, which is more pronounced than in the experiments.

The absence of smoothing effect of the fluid viscosity on the pressure rise in a shock wave seems to be partially responsible for the overestimation of pressure unsteadiness. Moreover, the flow pattern at 85% span, close to the trailing edge is affected by the tip clearance, as indicated by the stage simulations by Michelassi et al. (2001). As a consequence a significant mass can flow from pressure to suction side, thereby decreasing the blade load and, ultimately, increasing the minimum pressure level on the suction side TE.

Figure 8 reports the pitch-wise unsteady averaged quantities obtained with the inviscid simulations. The axial flow angle distribution at the rotor blade exit is compared with both experimental data and the results obtained from a NISRE computation (from Dènos et al. 1999) in which losses are evenly distributed along the rotor span. The agreement between the NISRE approach and the unsteady averaged profiles is good. This is not surprising since both approaches do not predict any sort of secondary flow. Actually the waving shape of the measured exit flow angle is due to the combined effect of various secondary effects, mainly the presence of the blade passage vortex and tip-hub horse shoe vortices.

Figure 8a also shows that the secondary flows penetrate quite close to the rotor mid-span, as proved by the deviation from the nominal exit flow angle (12-deg at mid-span). Figure 8b compares the experimental time and pitch-wise-averaged total temperature distribution with the unsteady numerical results. For radial position above 0.4 the total temperature profile is followed closely, but the absence of secondary effects in the calculations provokes a nearly constant total temperaure distribution which is far from experiments close to the root portion of the blade. On account of what seen for the exit flow angle, this disagreement is not surprising. Still the unsteady simulations demonstrate that the mid-span value of the total pressure is remarkably well reproduced, thereby proving the existence of a nearly two-dimensional flow portion around the rotor blade. The agreement with the NISRE calculations are good, although both are not able to reproduce the correct total temperature profile which, as seen for the exit flow angle, is strongly affected by secondary flows which, while governing the exit flow angle, can alter the local extraction of energy. Globally the integral value of the inviscid total temperatures is in good agreement with the experimental data and NISRE estimate, allowing a reasonable forecast of energy exchanges. Near hub, where secondary flows and wall boundary layers are well developed, the accuracy of the unsteady computation is similar to that obtained with the NISRE approach.

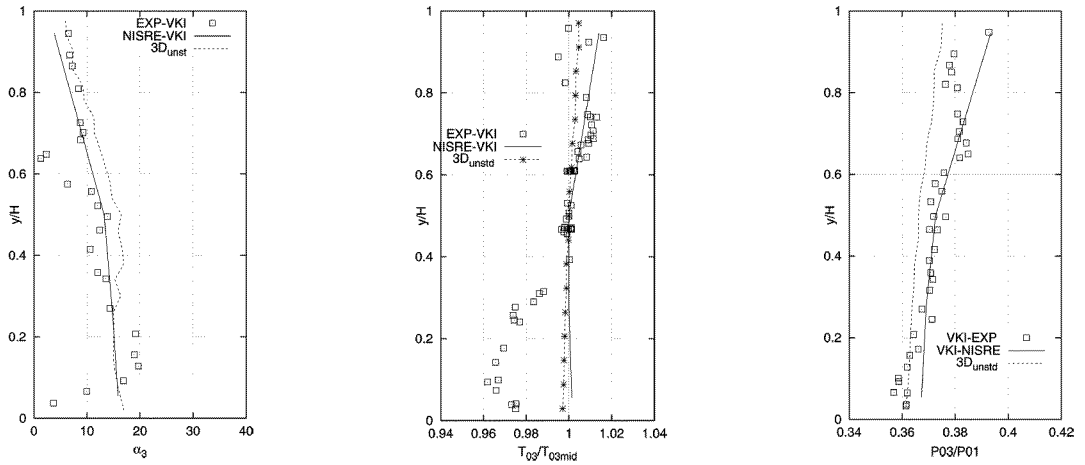

a) Averaged Alfa Flow angle **b) Averaged Total Temperature** **c) Averaged Total Pressure**

Figure 8: Pitch-wise Averaged Quantities

The total pressure profiles shown in figure 8c allow the same conclusions to be drawn. The time averaged values stemming from the unsteady inviscid calculations follow the experimental results with better accuracy, especially in the lower part of the blade in spite of some inaccuracies connected to the inviscid approximation. The capability of the unsteady approach to model the time

dependent flow should be checked by the analysis of the frequency spectrum. Instantaneous pressure has been monitored for several representative points located along rotor and stator blade surface (Denos et. al., 1999, Figure 18-a).

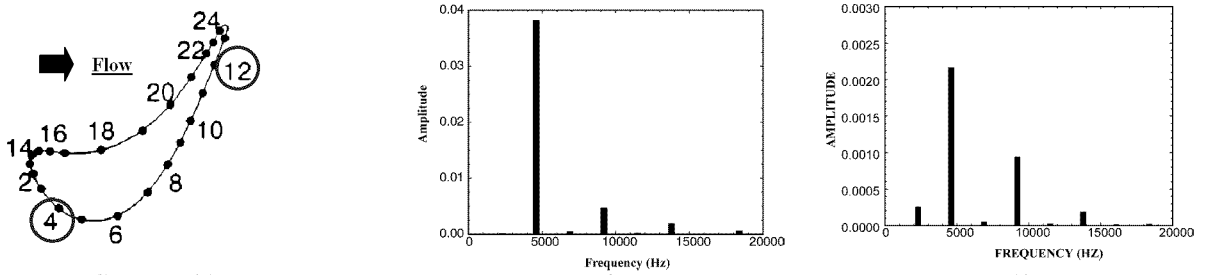

a) Rotor Gauge Position **b) Rotor LE gauge 4** **c) Rotor TE gauge 12**

Figure 9: Frequency Spectrum

The frequency analysis for two points located near LE and TE of rotor blade on suction surface are reported in Figure 9. For both gauges the main harmonic observed is the stator blades passing frequency. These basic frequencies of the spectrum (figures 18-b and 18-c) can be computed from the speed rotation (6500 RPM) and the blade count ratio (2:3) leading to a main peaks at f=4.66 kHz and the corresponding multiples (9.32 kHz, 13.98 kHz …). The remarkable amplitude of the first harmonic at LE is due both to the not uniform exit flow field from the stator blades (mainly due to the presence of vane TE shock impinging on the rotor) and to the small gap existing between the stator TE and the rotor LE. The amplitude of the pressure discontinuity varies considerably depending on the location on the rotor blade. The maximum amplitude is at gauge 4 because directly heat by the shock wave. Flowing toward the TE, the pressure fluctuations are strongly reduced (two orders) by the action of the vane acceleration effect, as can be observed in figure 9-c.

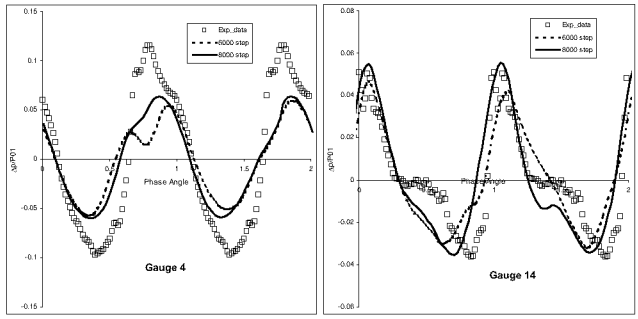

Figure 10: Unsteady Pressure Fluctuations

Figure 10 shows the unsteady pressure fluctuations $\Delta p/P01 = (p - p_{averaged})/P01$ for two rotor blade locations at mid-span. The two selected points lay on the suction side at approximately 20% axial chord (again point 4 in Figure 9) and on the leading edge (point 14). On the axis the phase spans from 0 to 2 while a complete periodic passage is completed (e.g. 2 NGV vanes and 3 rotor blades). The experimental data have been described by Dènos et al., 2000, who proposed a detailed interpretation of the flow in the stator/rotor gap. In the experiments pressure traces on gauge 4 clearly indicate high amplitude fluctuations in the rotor LE region, related to the passage of the vane TE fish tale shock (periodically oscillating around the axial direction from about +20° to –20°). In the same Figure two time-accurate computations, are compared with the experimental unsteady profile, obtained doubling the number of time steps during the unsteady simulation and the accuracy seems to improve with the increasing time resolution. The basic feature of the instantaneous signal are reproduced by the numerical results even if peak amplitudes of pressure fluctuations are under predicted mainly at gauge 4. Anyway in this point the under estimation behaves coherently with the pressure disagreement already observed at the same station in the averaged profiles of Figures 7. Moreover, in this location the stator wake hits the rotor blade almost tangentially (Michelassi et al.,

1999). This could provoke a complex interaction between the rotor boundary layer and the stator wake, which is clearly governed by viscous effects.

Viscous results

The time-averaged static pressure profiles on the rotor blade are reported in Figure 11 against curvilinear abscissa, for the same radial sections of Figure 7. The agreement with experiments at 50% span on pressure side confirms the in-viscid results. On the suction side the under prediction of flow acceleration is still present confirming the slight underestimation of the incidence but the pressure distribution of the experimental results near the shock location is more accurately followed.

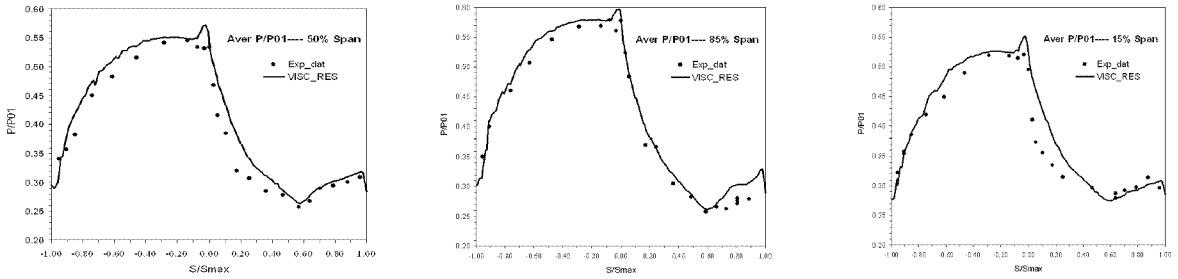

a) Averaged rotor pressure - 50% span **b) Averaged rotor pressure - 15% span** **c) Averaged rotor pressure - 85% span**

Figure 11: Time averaged Pressure Profiles

As expected in the viscous computation the up-down shape shown in the in viscid assumption disappeared due to the presence of smoothing effect of the fluid viscosity on the level of acceleration and recompression in correspondence of some relative positions of the two rows. Also the strong acceleration of the flow on the suction side close to the rotor trailing edge at tip and hub disappeared (Figures 11a and 11b), according to the more accurate physical assumption and the agreement with experimental results is improved.

Phenomena such secondary flow development inside the stator blade and their evolution in the rotor blade, depending on the relative blade position between rotor and stator and the blade wakes development have a deep impact on loss profile and distribution and thus on the whole turbomachine performances.

The viscous approximation can provide an useful tool for the basic understanding of such phenomena. In this regard in Figure 11.b the entropy contours at the stator exit are shown in axial plane 1, situated at 10 % of the axial chord downstream the stator TE. The stator wake is well outlined by the high loss region in the middle of the area.

As can be noticed the mid-span flow is essentially 2D, most of the loss being confined in the blade wake. Near hub and tip other high loss areas (1) can be underlined due to the development of wall boundary layers in the stator channel. The extension and thickness is small in comparison to the radial and pitchwise extension of the blade, limiting their influence in the regions very close to solid surfaces. As expected the boundary layer growth doesn't seem to affect the core of the flow, which remains almost undisturbed.

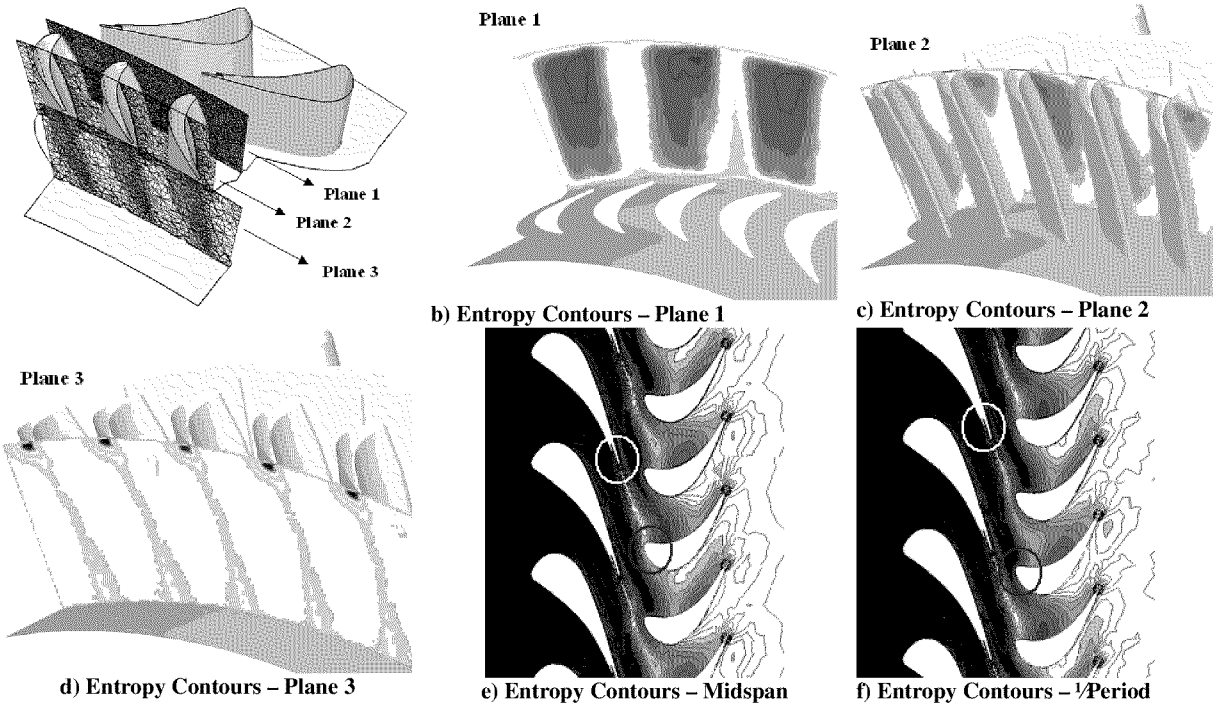

Figure 12: Entropy Contours

In Figure 12 e the entropy contours at 50% span are shown and the TE wakes can be clearly identified. These contours confirm that the entropy production in the NGV is essentially provoked by the SS boundary layer that grows until the final part of the blade, detaches in correspondence of the stator TE region, diffuses and finally impinges on the rotor blade. On the pressure side the boundary layer is almost invisible till the LE is reached, due to favourable pressure gradient experienced by the flow field in most of wall surface. On this side of the blade the more relevant loss seems to be represented by the mixing process between coolant injection and the main flow downstream the TE, responsible for the second high loss stripe of the wake. The shape of the wake from the NGV is almost independent from the relative position between the two rows while losses in the main core of the flow are not evident. When the wake moves toward the rotor blade the effect on the flow can be different depending on the relative position of the two rows. For instance in figure 12.e the wake impinges on the LE of the blade and is split in two different branches, the first one on the PS and the second on the SS. After a half period the wake impinges directly on the blade PS effecting primarily the SS flow on the LE.

In figure 12.d the entropy carpet plot is shown for reference plane 3, located downstream the rotor blade TE for tangential position corresponding to that of fig 12.e. In this plane high loss regions can be clearly identified corresponding to the rotor blade wake. Near the tip entropy production bubbles can be detected according to the combined effect of the tip leakage vortex and shroud boundary layer that are both contributing to the secondary flows in this region.

The ad hoc grid refinement performed for viscous computations in this area were necessary for the more accurate description of the viscous boundary layer profile and the velocity distribution. The shape and the distribution of the high loss region appears to be quite dependent on the relative row positions of the stator/rotor rows. Deep discussion of the results could be possible but is out of the scope of this paper intended to report mainly the challenge and the effort required in solving the unsteady flow field in real stage configuration.

6. CONCLUSIONS

A 3D unsteady solver has been discussed in the viscous and in-viscid assumption through the comparison against experiments. The peculiar aspect of the present application, compared to documented works, is given by the completely hybrid-unstructured nature of the approach. This

feature allows an easy and flexible representation of the stage in view of future more detailed flow investigations, as required by viscous simulations or shock interactions, and of more complex geometry as required by cooling systems or by row leakages.

The use of unstructured grids posed new difficulties for the matching of the stator/rotor rows, which have been here overcome by a crude but general and automatic linear interpolation strategy, but on the other hand offers a great flexibility in the grid generation and modelling with substantial reduction in the grid points demand. The potential stator rotor interaction has been reproduced with a satisfactory accuracy demonstrating that the unsteady Euler approach allows a more realistic description in comparison to steady state computations of the flow pattern, especially in the presence of physical phenomena such unsteady shock interaction which can not be accounted by in a steady assumption.

In order to have a deeper insight of phenomena concerning the periodic evolution of the NGV wakes, tip vortex structures and the effect of unsteadiness on the global stage efficiency, a more accurate analysis , based on full viscous, calculation was required. Viscous calculation on the other hand posed serious problems for the management of the data file and the CPU usage. To accurately reproduce those viscous effects more stringent requirements were imposed on the grid cell dimension especially near boundary layers in the solid surfaces at hub tip and blade profile. The grid dimensions typical of a realistic viscous computations (about 1.8 ML node elements) created difficulties for the management and storage of the input and output data required or produced during the processing of the solution and compelled the complete reconsideration of all the phases involved in the CFD solution and the optimisation of all the pre and post processing routines. The most advanced programming tools such Fortran 90 dynamic memory allocation and de-allocation of unused matrices were necessary for the full storage of geometry, exceeding the capacity of local workstation. Efficient interpolation techniques and a rationale use of the I/O management were necessary to reduce the length of the grid sequencing technique and all the post processing phases of the results management. In conclusion great effort have been successfully carried out on the different aspects of the calculation to face correctly and profitable the challenge to compute and investigate unsteady flow in a full turbine stage.

ACKNOWLEDGMENTS

The present research was carried out under contract for the European Commission as part of the Brite-EuRam TATEF (Trubine Aero-Thermal External Flow) project (BRPR-CT97-0519). The authors wish to acknowledge Dr. Ing. Paolo Malfetti and CINECA for the tests on the Origin3k and for the active support in the parallel solver porting.

REFERENCES

Adami P., Martelli F. and Michelassi V., 2000, "Three-Dimensional Investigations for Axial Turbines by an Implicit Unstructured Multi-block Flow Solver", ASME, IGTI TurboExpo 2000, Munich.

Adami P., Michelassi, V., Martelli, F., 1998 "Performances of a Newton-Krylov scheme against implicit and multi-grid solvers for inviscid flows" AIAA paper 98-2429.

Adami, P., 1999 "Computations for internal flows with a low-mach preconditioned Newton-Krylov scheme", 3rd European Conference on Turbomachinery. London.

Barth, T.J.,1991 "Numerical Aspects of Computing Viscous High-Reynolds Number Flows on Unstructured Meshes", AIAA Paper 91-0721, Jan.

Belardini E., Adami P., Martelli F. "*Development of an Unsteady Parallel Approach for 3D Stator-Rotor Interaction*" 4th European Conference on Turbomachinery, Fluid Dynamics and Thermodynamics- Firenze 20-23 March 2001, IMechE Journal of Power and Energy2001- Vol.215. n.A6.

Dawes, W.N., 1992, "The Simulation of Three-Dimensional Viscous Flow in Turbomachinery Geometries Using a Solution-Adaptive Unstructured Mesh Methodology" Transaction of ASME Vol. 114, July.

Dawes, W.N., 1994, "A Numerical Study of the Interaction of a Transonic Compressor Rotor Overtip Leakage Vortex with the Following Stator Blade Row", ASME Paper 94-GT-156.

Dénos R., Sieverding C.H., Arts T., Brouckaert J.F. and Paniagua G., 1999, "Experimental Investigation of the Unsteady Rotor Aerodynamics of a Transonic Turbine Stage", 3rd European Conference on Turbomachinery. London.

Denos, R., Arts, T., Paniagua G., Michelassi, V. and Martelli, F., 2000, "Investigation of the unsteady Rotor Aerodinamics in a Transonic Turbine Stage" 2000-GT-435.

Dorney D.J. and Sharma O.P., 1997, "Evaluation of Flow Field Approximations for Transonic Compressor Stages", J of Turbomeachinery, Vol. 119.

Gallus H.E., Zeschky J. and Hah C., 1994, "Endwall and Unsteady Flow Phenomena in an Axial Turbine Stage" ASME 94-GT-143.

Giles, M. B., 1990, "Stator/Rotor Interaction in a Transonic Turbine" AIAA J. of Propulsion, Vol. 6, No. 5.

Hah C., Copenhaver W.W. and Puterbaugh S.L., 1993, "Unsteady Aerodynamic Flow Phenomena in a Transonic Compressor Stage", AIAA-93-1868.

Haselbacher, A., McGuirk, J.J., Page, G.J., 1999, "Finite Volume Discretization Aspects for Viscous Flows on Mixed Unstructured Grids" AIAA J., Vol. 37, No. 2.

He L.,1996,"Time Marching Calculations of Unsteady Flows, Blade Row Interaction and Flutter", VKI-LS 1996-05.

Kwon, O.J. and Hah, C., 1995, "Simulation of Three-Dimensional Turbulent Flows on Unstructured Meshes" AIAA J. Vol.33, No. 6, June.

M. Von Hoyningen-Huene, A. R. Jung, 2000, "Comparison of Different Acceleration techniques and methods for Periodic Boundary Treatment in Unsteady Turbine Stage Flow Simulations" J. of Turbomachinery, Vol. 122.

Mavriplis D.J. 1995, "Three-Dimensional Multigrid Reynolds Averaged Navier Stokes Solver for Unstructured Meshes" AIAA J., Vol.33, No. 3.

Martelli, F. Adami, P. Belardini, E, "Unsteady Rotor/Stator Interaction : An Improved Unstructured Approach" 46th ASME International Gas Turbine & Aeroengine Technical Congress June 4-7, 2001, N.Orleans, Louisiana, USA

Michelassi, V, Martelli, Denos, R., Arts, T., Sieverding, C.H. 1999 "Unsteady Heat Transfer in Stator-Rotor Interaction by Two-Equations Turbulence Model" J. Turbomachinery,July.

Michelassi, V., Giangiacomo, P., Martelli, F., Dénos, R., Paniagua, G., "Steady three-dimensional simulation of transonic axial turbine stage", offered for IGTI-2001.

Pulliam T.,H., Rogers, S., Barth, T., 1996, "Practical Aspects of Krylov Subspace Iterative Methods in CFD", *Prog. and Challenges in CFD Methods and Algorithms*, Seville, AGARD CP-578.

Rai, M., M., 1989, "Three-Dimensional navier-Stokes Simulations of Turbine Rotor-Stator Interaction; Part I-Methodology" AIAA J. of Propulsion, Vol. 5, No. 3 May-June.

Roe P.L., 1986 "Characteristic based scheme for Euler equations" , Ann. Rev. Fluid Mech., 18.

Saad, Y., 1994 "Krylov Subspace Thechniques, Coniugate Gradients, Preconditioning and Sparse Matrix Solvers", CFD VKI LS 1994-05 VonKarman Institute for Fluid Dynamics.

Saad, Y., 1994, "Krylov Subspace Techniques, Coniugate Gradients, Preconditioning and Sparse Matrix Solvers", CFD VKI LS 1994-05 VonKarman Institute for Fluid Dynamics.

Sayma A. I., Vahdati M., Sbardella L., and M. Imregun, 2000, "Modeling of the Three-Dimensional Viscous Compressible Turbomachinery Flows Using Unstructured Hybrid Grids" AIAA J. Vol. 38, No. 6.

Sharma O.P., Pickett G.F. and Ni R.H., 1992, "Assessment of Unsteady Flows in Turbines", J. of Turbom. Vol. 114.

Slack, D.,C., Whitaker, D.,L., Walters, R.,W., 1994, "Time Integration Algorithms for the Two-Dimensional Euler Equations on Unstructured Meshes", AIAA J. Vol. 32, No. 6.

Venkatakrishnan, V., 1995, "A Perspective on Unstructured Grid flow Solvers", Technical report AIAA Paper 95-0667, AIAA 33rd Aerospace Sciences Conference, Reno.

Walraevens R.E., Gallus H.E., Jung A.R., Mayer F.J. and Stetter H., 1998, "Experimental and Computational Study of the Unsteady Flow in a 1.5 Stage Axial Turbine with Emphasis on the Secondary Flows in the Second Stator" ASME Paper 98-GT-254.

Centaur™ -Grid Generation Software Package Distributed by CentaurSoft (web site www.centaursoft.com)

Paper #37
Discussor's name A. Soulaimani
Author F. Martelli

Q: 1) Since the precondition and its factorization take most of the CPU time, do you compute it at every time step?
2) You can save a substantial amount of computing time if you freeze it for a few time steps (2-5) steps). I am sure of the result!

A: 1) Yes
2) Okay